NEUROSCIENCE

Sequential maturation of stimulus-specific adaptation in the mouse lemniscal auditory system

Patricia Valerio, Julien Rechenmann, Suyash Joshi, Gioia De Franceschi†, Tania Rinaldi Barkat*

Stimulus-specific adaptation (SSA), the reduction of neural activity to a common stimulus that does not generalize to other, rare stimuli, is an essential property of our brain. Although well characterized in adults, it is still unknown how it develops during adolescence and what neuronal circuits are involved. Using in vivo electrophysiology and optogenetics in the lemniscal pathway of the mouse auditory system, we observed SSA to be stable from postnatal day 20 (P20) in the inferior colliculus, to develop until P30 in the auditory thalamus and even later in the primary auditory cortex (A1). We found this maturation process to be experience-dependent in A1 but not in thalamus and to be related to alterations in deep but not input layers of A1. We also identified corticothalamic projections to be implicated in thalamic SSA development. Together, our results reveal different circuits underlying the sequential SSA maturation and provide a unique perspective to understand predictive coding and surprise across sensory systems.

INTRODUCTION

We are constantly exposed to unexpected events. The capability to identify them is crucial for survival and allows, for example, avoiding threats and remaining safe. But how are surprising stimuli detected in the first place? An essential task for the brain is to distinguish these deviant stimuli from common ones, a process described as stimulus-specific adaptation (SSA). In the auditory system, the reduction of neural activity as regularity is established and has been studied in the mature brain of humans (*1*–*3*) and animals, such as rodents (*4*–*6*), cats (*7*), and songbirds (*8*). SSA has most commonly been characterized using an oddball paradigm, comprising sequences of common (standard) and rare (deviant) stimuli, where the number of preceding standard tones to a deviant tone varies. These studies associated two mechanisms with SSA: repetition suppression or adaptation, and prediction error (PE) or "true" deviance detection. While repetition suppression refers to the decrease in response to a repeated stimulus, PE is defined through an increase in response to the deviant sound compared to its standard response that cannot be explained by repetition suppression (*5*). Together, these two mechanisms explain a decreased response to the standard sound that does not, or only partially, generalize to the deviant sound, combining PE and repetition suppression of the standard tone (*6*).

Auditory SSA was first identified in the auditory cortex (ACx) of anesthetized cats (*9*). It was later described in the auditory thalamus [medial geniculate body (MGB)] (*7*) and the inferior colliculus (IC) (*10*) but was not found in other auditory nuclei besides these three areas of the central auditory system (*11*). Researchers have characterized SSA for pure frequency tones, white noise (WN), and, more recently, tone clouds (*12*–*14*). A study also identified SSA for more complex sounds, such as animal vocalizations (*15*). At the cellular level, studies have found SSA to depend on functional properties of auditory cells, such as best frequency (BF) and bandwidth, as well as stimulus features, such as octave distance between standard and deviant, sound level, and probability or repetition rate of both tones (*16*–*18*).

Department of Biomedicine, Basel University, 4056 Basel, Switzerland.
*Corresponding author. Email: tania.barkat@unibas.ch
†Present address: Epigenetics and Neurobiology Unit, EMBL Rome, Via Ramarini 32, 00015 Monterotondo, Italy.

The auditory pathway is characterized by feedforward and feedback neuronal projections between IC, MGB, and primary ACx (A1). In the feedforward or lemniscal pathway, the central part of IC (ICC) projects to the ventral part of MGB (MGV), which then projects via thalamocortical connections to the A1 input layer 4 (L4) (*19*–*21*). Intracortical connectivity in A1 occurs between L4 and superficial (L1 and L2/3) and deep (L5 and L6) layers (*22*). In the feedback pathway, A1 L5 and L6 send projections to downstream areas via corticofugal connections, including MGB (corticothalamic) and IC (corticocollicular) (*23*–*27*). These descending projections from ACx have been studied as regulators of SSA. Previous studies focused on the corticothalamic circuits and showed that inactivation of the ACx does not ablate the appearance of SSA but instead decreases the surprising effect in MGB (*4*, *28*). For corticocollicular projections, similar results were identified, with SSA decreased in IC upon inhibition of the ACx (*29*, *30*). These results indicate that ACx is not required to generate SSA but might regulate it through a gain modulation mechanism.

SSA has been extensively characterized in adulthood (*5*, *6*, *10*, *30*, *31*). It is, however, still unknown whether it changes during development. This knowledge, in addition to informing about how SSA changes with brain maturation and experience, would help identifying and dissecting the different mechanisms involved. Thus, this study aimed at exploring SSA during the juvenile development, from postnatal day 20 (P20) to adulthood (≥P50), in the lemniscal pathway of the mouse central auditory system (A1, MGV, and ICC). We used in vivo electrophysiological recordings while passively exposing awake mice to an oddball sequence paradigm and found that SSA sequentially matures in ICC, then in MGV, and lastly in A1. These changes in maturation cannot be explained solely by changes in adaptation, suggesting that PE plays a prominent role. In addition, A1 SSA alterations are experience-dependent and observed in the neuronal circuits of its deep but not input layers. We further found MGV to be regulated by corticothalamic projections during this adolescent development period. Last, video-monitoring the mice during passive exposure to the oddball paradigm allowed us to identify an ear movement associated with the sound presentation. However, this response was not different between deviant and standard tones nor across ages, suggesting that the response to the deviant is more than a reflex-like response. Together, our findings reveal a sequential maturation of SSA in the central auditory system and identify different mechanisms underlying it.

RESULTS

SSA matures sequentially along the central auditory system

To study SSA in the central auditory system during juvenile development, we used single or multishank, 32- or 64-channel silicon probes to perform acute extracellular recordings in the central auditory areas of awake wild-type mice with ages ranging from P20 to P50 (Fig. 1, A to C). ICC, MGV, and A1 were identified on the basis of their functional tonotopy (fig. S1, A, B, D, E, G, and H) and anatomically confirmed (fig. S1, C, F, and I). We used an oddball paradigm with 10 different sequences in which the number of standards preceding a deviant pure frequency tone varied from 1 to 10 (see Materials and Methods). We defined the frequency of the standard (f_1) and deviant (f_2) tones at 0.5 octave distance from each other around the BF of a strongly responding unit in each penetration (see Materials and Methods). To evaluate whether the responses to these tones differ across frequencies, f_1 and f_2 were swapped for a second trial of the protocol, where f_2 was the standard and f_1 was the deviant tones (Fig. 1D).

We extracted the spike rate in response to standard and deviant tones from recorded single and multiunits by averaging the 15 repetitions of each sequence and then all 10 sequences (Fig. 1E and see Materials and Methods). The evoked responses in a 60-ms time window from tone onset were used for the analysis. We first calculated the SSA index {SI f_i = [DT(f_i) − ST(f_i)] / [DT(f_i) + ST(f_i)], where DT is the deviant tone and ST is the standard tone response} (see Materials and Methods) for f_1 and f_2 (fig. S2A). SI values vary from −1 to 1 (fig. S2B; −1 to 0, stronger response to standard tone; 0, equal response to both tones; 0 to 1, stronger response to deviant tone). To avoid biases due to the choice of f_1 and f_2 and to specifically study SSA, we selected units showing a stronger response to the deviant than to the standard condition for both f_1 and f_2 (SI $f_1 > 0$). In ICC, neurons show a weak SSA across the ages studied (P20 to P50), with SI f_1 and SI f_2 values clustered close to 0. In MGV, P20 mice show a scattered distribution of SI values for both frequencies. However, at P30, P40, and P50, the values decrease. In A1, P20, P30, and P40 mice present a scattered SI distribution, and a clear decrease in SI values can only be found in P50 mice (fig. S2A).

To evaluate these results independently of the frequency, we calculated the common SI {CSI = [DT(f_1) + DT(f_2) − ST(f_1) − ST(f_2)] / [DT(f_1) + DT(f_2) + ST(f_1) + ST(f_2)]}, which summarizes the responses to f_1 and f_2 (see Materials and Methods). As observed for SI, ICC units have low deviance sensitivities (small CSIs), which do not change significantly across adolescence (Fig. 1F). In MGV, P20 units have a strong CSI. However, at P30, deviance sensitivity significantly decreases and stabilizes for the P40 and P50 groups (Fig. 1G). For A1 units, CSI is strong from P20 to P40 but significantly drops at P50, showing a decrease in deviance sensitivity at this later maturation stage (Fig. 1H).

When comparing the three areas per age group, ICC presents a significantly lower CSI compared to the other areas across ages. A1 presents similar (P20 and P50) or stronger (P30 and P40) CSI as compared to MGV (Fig. 1I). These results indicate a hierarchical SSA along the central auditory areas across adolescence as similarly shown in adulthood (*5*). We confirmed that these results were not due to our selection of units with SI $f_i > 0$, as the results were similar when including all units (including those with SI $f_i < 0$; fig. S2B) or when removing units responding to a frequency only in the deviant and not in the standard position (SI $f_i = 1$; fig. S2C). The results were not sex specific (fig. S2, D and E). We also verified that these changes in CSI were not due to different neuronal sampling among the different age groups or areas (fig. S3, A and B) nor choice of f_1 and f_2 (BF distance to deviant; fig. S3C).

Together, our results show that the three central auditory areas process deviant sounds distinctly during adolescence. During this developmental phase, CSI decreases in MGV and A1 but not in ICC. Our data suggest an earlier development of ICC (<P20), whereas MGV refines until P30 and A1 later in time (≥P50), showing a sequential maturation of SSA across the central auditory system.

Adaptation of the responses to the standard does not fully explain the developmental changes of SSA

We have found decreases in SSA processed in MGV and A1 during mouse juvenile development. We next asked whether these changes depend on the adaptation of the responses to the standard or deviant tone across time. We plotted the responses across a recording session as a function of time, normalized them to the response of the first sound, and averaged the response across all neurons in a group (see Materials and Methods). It was clear that the adaptation to the standard happened within the first few trials of each session (975 trials) across ages and areas and that the difference between the steady-state responses of the standard and the deviant tones was larger in A1 than in MGV or ICC (Fig. 2A and fig. S4, A and B). We then fitted the standard or the deviant responses with a single exponential function and found that both the time constants (tau) and the asymptotes (coefficient *a*) were changing significantly across age groups (fig. S4, A to D). However, these changes cannot fully explain the changes observed in SSA (Fig. 1, F to H) and could, therefore, not by themselves explain the maturation trajectories of SSA across development. It is of note that the data were not well fitted by a single exponential function as reflected in the low r^2 values, suggesting that neurons have multiple timescales of adaptation as previously observed (*31*).

We performed another analysis to address the possible role of this adaptation in the developmetnal trajectory of CSI. As the adaptation happened within the first few trials of each session, we removed the first repetitions of each sequences (corresponding to 65 tones or the first 22.7 s of each session; see Materials and Methods) when most of the adaptation happens and reanalyzed the CSI. The results show the same developmental changes of CSI for ICC, MGV, and A1 (fig. S4E), suggesting again that adaptation cannot explain the developmental changes and that another mechanism must be at play.

We then asked whether the responses to the standard or the deviant within a sequence were dependent on the number of preceding standards. To answer this question, we calculated the averaged spike rate of response according to the tones' sequence position (Fig. 2B and see Materials and Methods). We normalized each value to the one obtained for the sequence with a single standard (i.e., number of preceding standard = 1 for deviant and 0 for standard; Fig. 2, C and D). Our results show an increase in response to the deviant with the number of preceding standard (Fig. 2C), whereas the response to the standard does not change across the sequences (0 to 9 preceding standards) and ages (Fig. 2D). Contrary to previous studies where increasing the number of preceding standards causes an adaptation to this tone (*10*, *12*, *17*, *18*), our data do not show a decrease in response relative to the number of preceding standards across a session. The differences among studies are probably due to the characteristics of the oddball paradigm, such as the length of the protocol, the number of repetitions of each sequence, the frequency of the sound stimulation, or the sound level used. Together, our data show that the

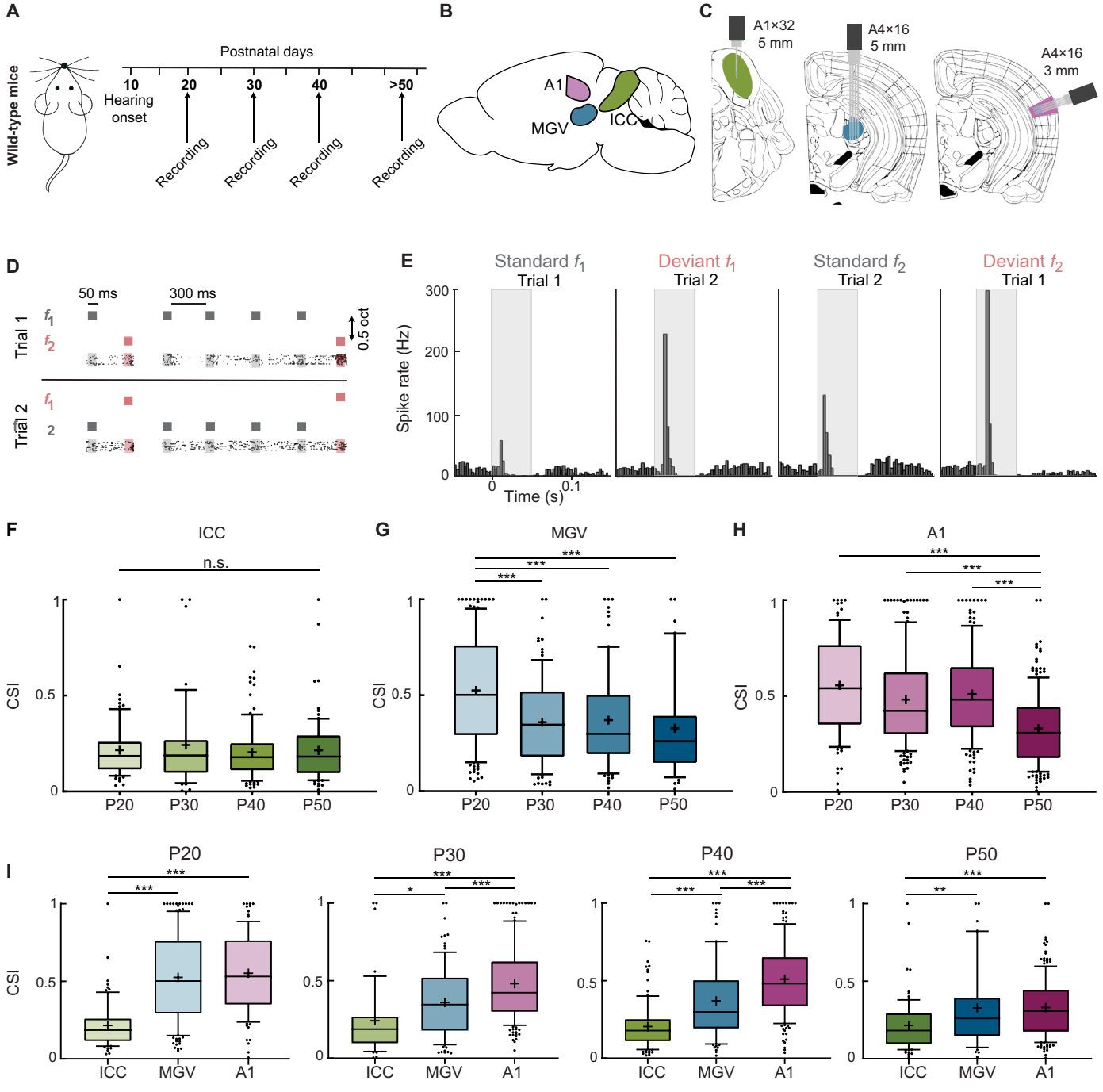

Fig. 1. SSA matures sequentially along the central auditory system. (**A**) Schematic of mouse development with time points of hearing onset and electrophysiological recordings. (**B**) Schematic of mouse brain with the location of the ICC (green), MGV (blue), and A1 (pink). (**C**) Schematic of coronal slice location of ICC, MGV, and A1 with recording electrodes. (**D**) Schematic of oddball sequence paradigm. Representative example of 2 of the 10 sequences and corresponding raster plots of an example P20 MGV unit—1 and 4 standards (gray) preceding a deviant (magenta) tone. (**E**) Representative peristimulus time histogram of an MGV P20 unit's response to the standard and deviant tone f_1 or f_2 for trials 1 and 2 (CSI = 0.344). (**F** to **H**) Average CSI for ICC, MGV, and A1, respectively. ICC: P20, 5 mice, 71 units; P30, 5 mice, 44 units; P40, 5 mice, 106 units; P50, 6 mice, 82 units; $f = 0.51$, df = 302. MGV: P20, 5 mice, 140 units; P30, 6 mice, 95 units; P40, 5 mice, 87 units; P50, 5 mice, 43 units; $f = 12.58$, df = 364. A1: P20, 7 mice, 96 units; P30, 6 mice, 183 units; P40, 5 mice, 154 units; P50, 7 mice, 183 units; $f = 28.05$, df = 615. One-way analysis of variance (ANOVA) with multiple comparisons. n.s., $P \geq 0.05$; ***$P < 0.0001$. (**I**) CSI for ICC, MGV, and A1 across P20, P30, P40, and P50 ages. P20: ICC versus MGV/A1, $f = 46.83$, df = 309. P30: ICC versus MGV, $f = 20.97$, df = 321. P40: ICC versus MGV/A1, $f = 62.75$, df = 346. P50: ICC versus MGV, $f = 10.39$, df = 307. Ordinary one-way ANOVA with multiple comparisons. Numbers as in (F) to (H). ***$P < 0.001$; **$P = 0.007$; *$P = 0.022$. In the boxplots, lines represent median, 25th, and 75th percentiles, + represents mean, whiskers represent 10th and 90th percentiles, and points below or above the whiskers are drawn as individual points.

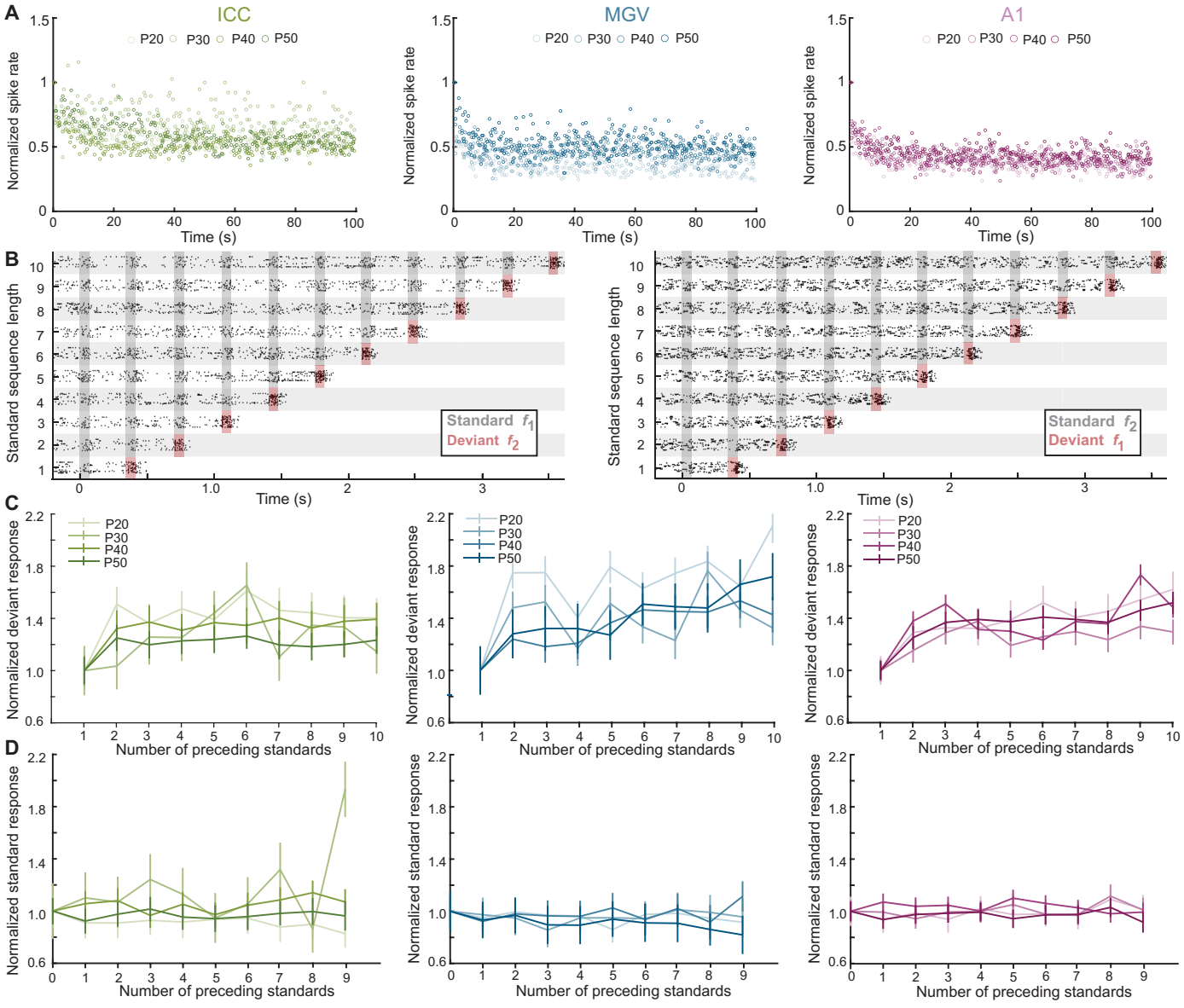

Fig. 2. Adaptation of the responses to the standard does not fully explain the developmental changes of SSA. (**A**) Average firing rate of the standard responses in the first 100 s of sessions, normalized to the first standard of the session. (**B**) Representative raster plot of a P20 MGV unit's response to the 10 oddball sequences with standard f_1 and deviant f_2 (left) and standard f_2 and deviant f_1 (right). (**C**) Normalized spike rate of response to the deviant tone f_2 for each number of preceding tones (2 to 10) to the single standard sequence (1). (**D**) Normalized spike rate of response to the standard tone f_2 for each number of preceding standards (1 to 9) to the single standard sequence (0). *n* as in Fig. 1 (F to H). Data represent means ± SEM.

changes in SSA during adolescence in MGV and A1 cannot be explained solely by the adaptation of the responses to the standard and support a possible prominent role of true deviance detection or PE (*5*, *6*, *30*).

SSA maturation does not correlate with changes in spontaneous activity, tuning bandwidth, or response threshold

As it has been shown that CSI depends on the functional properties of auditory neurons (*16*, *17*), we asked whether functional property changes during adolescence correlate with SSA maturation. In all our recordings, we exposed mice to pure tones of varying frequency and sound levels to determine the frequency response areas (FRAs) of each recorded unit (see Materials and Methods). We then extracted their different properties, including spontaneous activity, bandwidth at 60-dB sound pressure level (SPL), and response threshold.

We first compared the spontaneous activity of neurons in all three areas to determine whether it was changing across age and confirmed that this property remains similar during juvenile development (Fig. 3, A and B, and table S1). We then asked whether a unit's tuning bandwidth at 60-dB SPL changes across adolescence and, if yes, whether it correlates with changes in CSI. This parameter corresponds to the range of frequencies each unit responds to at 60-dB SPL. We found that bandwidth significantly increases in ICC at P40 and in A1 at P50,

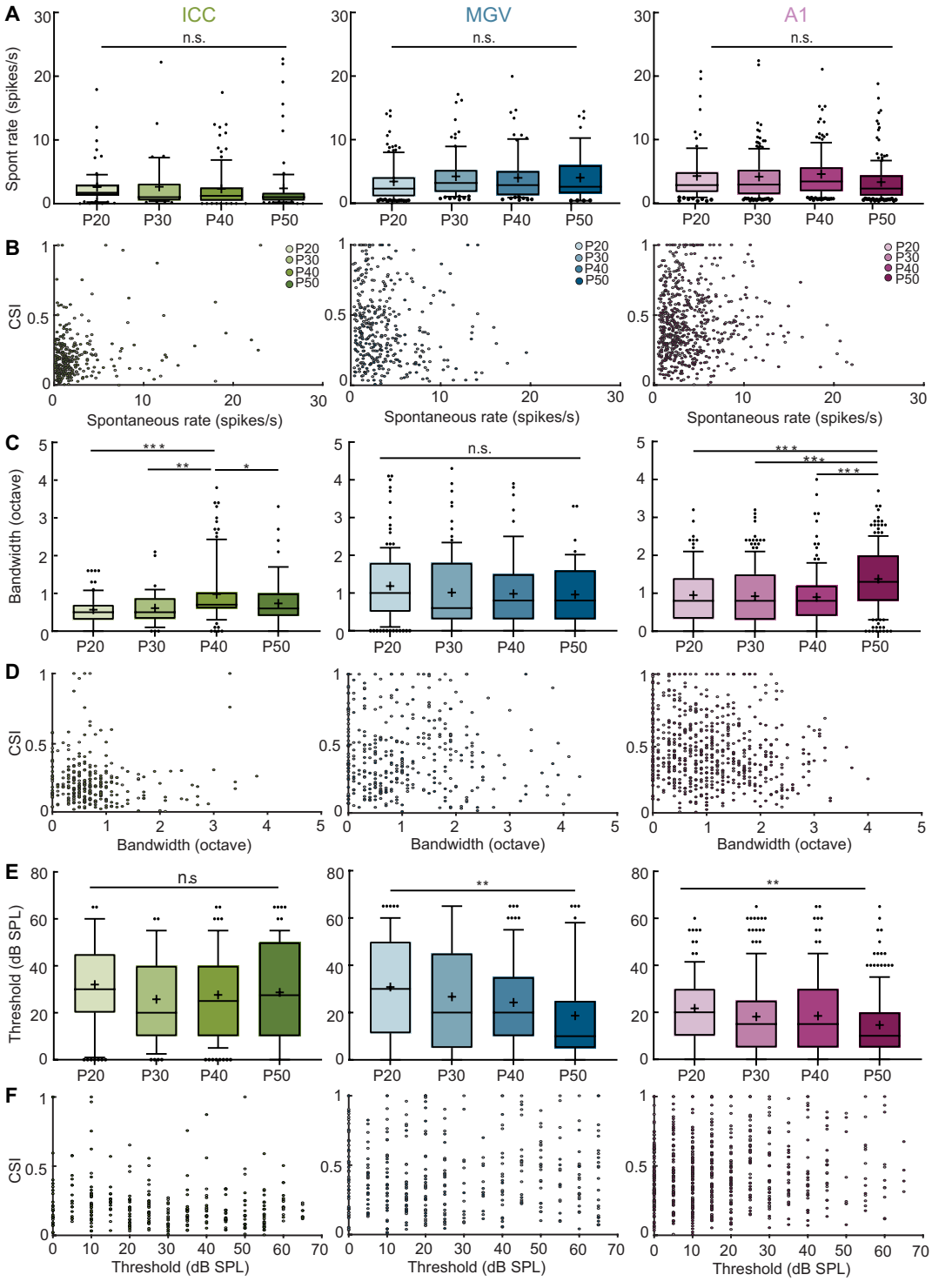

Fig. 3. SSA maturation does not correlate with changes in spontaneous activity, response bandwidth, or threshold. (**A**) Spontaneous activity across adolescence in ICC, MGV, and A1. n.s., $P > 0.05$, one-way ANOVA with multiple comparisons. ICC: $f = 0.14$, df = 302; MGV: $f = 0.91$, df = 364; A1: $f = 2.52$, df = 615. (**B**) Scatter plot of CSI versus spontaneous activity across brain areas. (**C**) Tuning bandwidth at 60-dB SPL across adolescence in ICC, MGV, and A1. ICC: P20 versus P40, $P = 0.0001$; P40 versus P50, $P = 0.0490$. P30 versus P40, $P = 0.0063$. MGV: n.s., $P > 0.05$. A1: P20 versus P50, $P = 0.0003$; P30 versus P50, $P < 0.0001$; P40 versus P50, $P < 0.0001$; one-way ANOVA with multiple comparisons. ICC: $f = 7.48$, df = 302; MGV: $f = 1.24$, df = 363; A1: $f = 14.52$, df = 603. (**D**) Scatter plot of CSI versus bandwidth across brain areas. (**E**) Response threshold across adolescence in ICC, MGV, and A1. ICC: n.s., $P > 0.05$. MGV: P20 versus P50, $P = 0.0043$. A1: P20 versus P50, $P = 0.0012$; one-way ANOVA with multiple comparisons. ICC: $f = 1.18$, df = 302; MGV: $f = 4.45$, df = 364; A1: $f = 4.68$, df = 615. (**F**) Scatter plot of CSI versus threshold across brain areas. For all panels, *n* as in Fig. 1. See table S1 for Pearson correlations of (B), (D), and (F). In the boxplots, lines represent median, 25th, and 75th percentiles, + represents mean, whiskers represent 10th and 90th percentiles, and points below or above the whiskers are drawn as individual points. *$P < 0.05$; **$P < 0.01$; ***$P < 0.001$.

while it stays stable otherwise (Fig. 3C). However, bandwidth does not correlate with CSI across all ages and nuclei studied (Fig. 3D and table S1), indicating that changes in bandwidth cannot explain the observed maturation in SSA.

We also characterized response threshold across adolescence. This parameter corresponds to the minimum sound level triggering a unit's response to a pure frequency tone. Although the threshold is stable in ICC, it decreases significantly in MGV and A1 during adolescence (between P20 and P50 groups; Fig. 3E). However, this decrease does not correlate with changes in CSI, neither in MGV nor in A1 (Fig. 3F and table S1). Together, our data indicate that SSA maturation does not relate to spontaneous activity, bandwidth, or threshold changes of the auditory neurons.

Auditory experience affects SSA maturation in A1 but not in MGV

It is known that experience strongly influences sensory processing. Preventing or masking sensory stimuli during development, such as dark rearing for the visual system (*32*, *33*) or exposure to continuous WN for the auditory system (*34*–*37*), affects how different processes mature in these sensory systems. As SSA matures in MGV and A1 during adolescence, we asked whether these changes could be experience-dependent. We first hypothesized that the decrease in CSI observed across development could be due to the natural exposure to sounds, thereby diminishing the surprise effect of a rarer sound. If this would be true, then decreasing auditory exposure would alter the maturation of SSA. To test this, we exposed mice to continuous WN from P20 to P50 (Fig. 4A and see Materials and Methods). Compared to the control P50 group, the WN-exposed P50 mice did not show any difference in the CSI values of MGV units (Fig. 4, B and C). However, A1 units showed a different outcome. WN exposure during adolescence prevented the decrease of deviance sensitivity at P50, with the exposed group showing CSI values closer to the younger control mice (Fig. 4, D and E).

We then asked the opposite and quantified SSA in mice overexposed to the surprising sounds during adolescence. Could an overexposure cause an adaptation to surprise and decrease the response to the deviant sound? We exposed mice to an oddball protocol with fixed f_1 and f_2 for 3 hours/day from P20 to P50, swapping f_1 and f_2 every day (Odd; Fig. 4F and see Materials and Methods). When the mice reached P50, we performed recordings in A1, while the mice were exposed to the oddball protocol with the same f_1 and f_2 as in the exposure. Contrary to what was expected, overexposure to surprising sounds during adolescence also prevented the decrease of SSA at P50 in A1, with the oddball-exposed group showing significantly larger CSI values than the control group (Fig. 4, G and H).

We also asked whether the exposures changed spontaneous activity, response bandwidth, or threshold. The WN-exposed mice did not show alterations in spontaneous activity, bandwidth, or threshold in MGV nor in bandwidth in A1, as compared to control mice. Although the response threshold in A1 was slightly decreased in WN-exposed mice, it was not correlated to CSI values (fig. S5, A to F, and table S1). In the oddball-exposed mice, the bandwidth was increased compared to control mice but again without any correlation to CSI values, whereas spontaneous activity and the response threshold were unchanged (fig. S5, G to I, and table S1).

Together, our results show that SSA maturation is experience-dependent in A1 but not in MGV, indicating that different mechanisms, one experience-dependent and one experience-independent, are involved in SSA. The diminution of structured sound exposure prevents the decrease in SSA at P50, but, unexpectedly, overexposure to these sounds also causes a large CSI during adulthood.

A1 SSA maturation is observed in deep but not input cortical layers

Our previous results show SSA maturation during adolescence in A1 and MGV. We also found this maturation to depend on earlier sound experience in A1. We then asked what the underlying causes at a circuit level could be and whether intracortical, thalamocortical (feedforward), or corticothalamic (feedback) connectivity differences during this developmental period could be involved (Fig. 5A). We first assessed whether the cortical changes in SSA depended on superficial, input, or deep layers (Fig. 5, B and C). To identify the different layers, we exposed mice to WN bursts while recording responses along the cortical column. We identified the laminar position of each unit through a current source density (CSD) analysis (see Materials and Methods) (*38*). Only the deep layers showed a significant decrease in CSI at P50, whereas this decrease was not observed in the input layer. In superficial layers, there was a tendency for a similar decrease, but it was not significant (Fig. 5D). However, the number of units recorded from these layers is low, and this tendency might be confirmed with higher numbers. For the exposed mice, both the WN and Odd groups showed significant differences with the control group in deep layers only (Fig. 5D).

We then asked whether the different cortical cell types express similar SSA maturation and divided our cortical units into two subpopulations: regular spiking (RS; putative excitatory and nonfast spiking) and narrow spiking (FS; putative fast spiking, parvalbumin-positive) neurons. We identified RS and FS neurons according to the peak-to-trough duration of their action potential waveform (Fig. 5E and see Materials and Methods) (*39*, *40*). This analysis was only possible in A1 since there are no inhibitory cells in MGV, and despite containing inhibitory neurons, there is no bimodal distribution of peak to trough in ICC (*19*). We then compared the CSI of RS and FS units. For both cell populations, CSI decreased at P50 and significantly increased in the P50 groups of WN- and Odd-exposed mice (Fig. 5F). We observed similar results for units belonging to the deep layers (Fig. 5G) and to the other layers, although the number of units in each subgroup was small.

Together, our results show that A1 SSA maturation depends on intracortical alterations of deep rather than input layers but not to one particular cell type. They suggest that intracortical circuits play a major role in the maturation of SSA. Since the input layers do not change significantly, our data also suggest thalamocortical projections to be already stable during this developmental period. However, as deep layers are the main output layers of the cortex, our findings indicate a possible implication of corticothalamic projections in the changes observed in MGV during adolescence.

Corticothalamic projections are implicated in SSA maturation

Following our previous results relating A1 SSA maturation to its deep layers, we asked whether the corticothalamic projections could play a role in the changes observed in MGV during adolescence. We coupled optogenetics to electrophysiological recordings in P20, P30, P40, and P50 mice to manipulate corticothalamic activity while quantifying CSI in MGV. We used a mouse line expressing channelrhodopsin 2 (ChR2) in parvalbumin (PV) positive cells to silence A1 while recording MGV

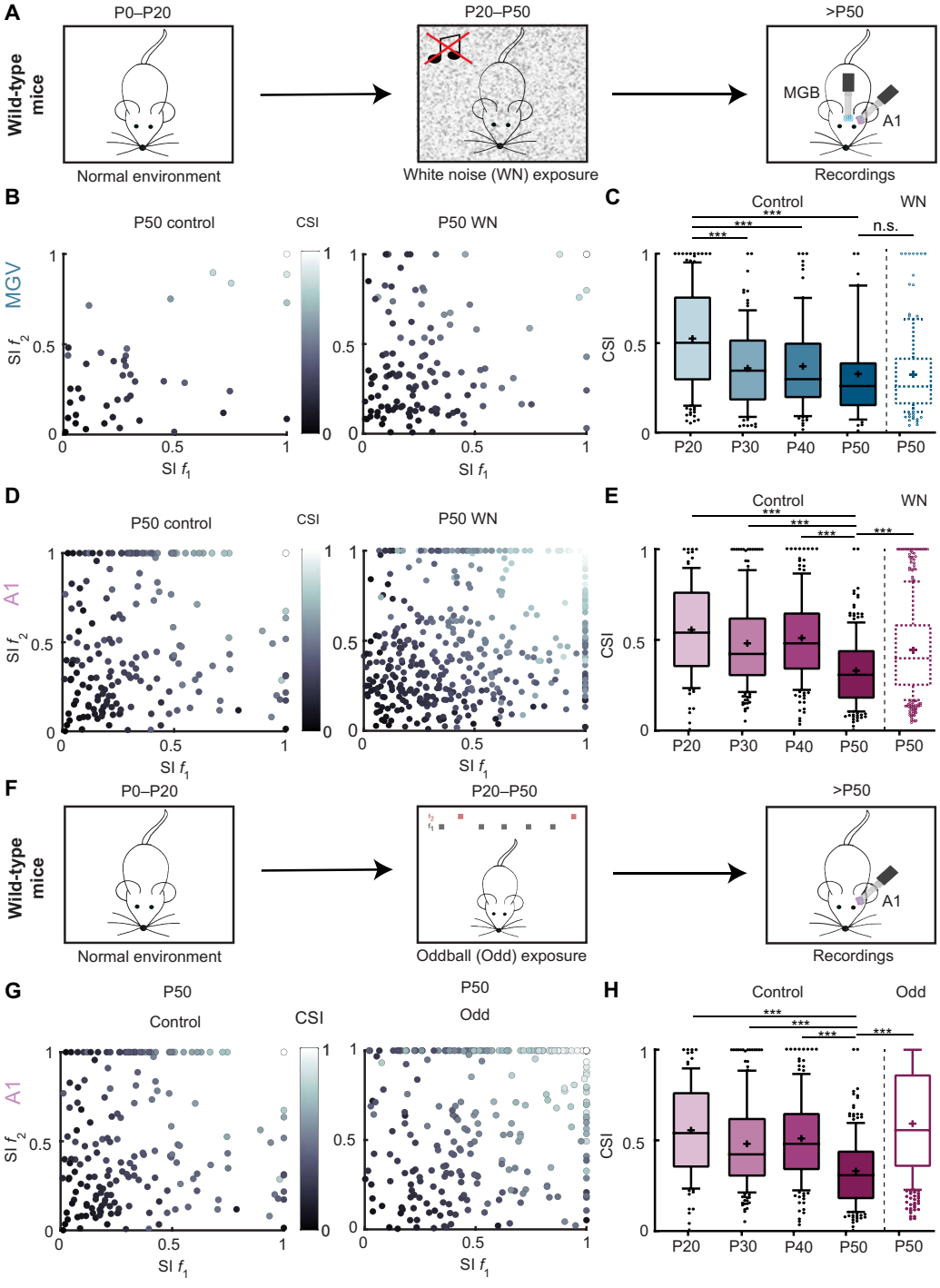

Fig. 4. Auditory experience affects SSA maturation in A1 but not in MGV. (**A**) Schematic of mouse postnatal development continuous WN exposure. P0 to P20, mice reared in normal acoustic environment; P20 to P50, exposure to continuous WN; after P50, MGV and A1 extracellular electrophysiological recordings. (**B**) Scatter plot of SI f_1 and SI f_2 for MGV P50 control (left; as in fig. S2A) and WN-exposed P50 (right). (**C**) Average CSI for control MGV P20, P30, P40, and P50 (*n* as in Fig. 1G) and WN-exposed P50 (5 mice, 132 units). Control P20 versus P30/P40/P50, ***$P < 0.0001$; control P50 versus WN P50, n.s., $P < 0.05$. (**D**) Scatter plot of SI f_1 and SI f_2 for A1 P50 control (left; *n* as in fig. S2A) and WN-exposed P50 (right). (**E**) Averaged CSI for control A1 P20, P30, P40, and P50 (*n* as in Fig. 1H) and WN-exposed P50 (7 mice, 448 units). Control P20/P30/P40 versus P50, ***$P < 0.0001$; control P50 versus WN P50, ***$P < 0.0001$. (**F**) Schematic of mouse postnatal development oddball (Odd) exposure. P0 to P20, mice reared in normal acoustic environment; P20 to P50, exposure to oddball paradigm with fixed f_1 and f_2; after P50, A1 extracellular electrophysiological recordings. (**G**) Scatter plot of SI f_1 and SI f_2 for A1 P50 control (left; as in fig. S2A) and Odd-exposed P50 (right). (**H**) Average CSI for control A1 P20, P30, P40, and P50 (*n* as in Fig. 1H) and Odd-exposed P50 (4 mice, 306 units). Control P20 versus P30/P40/P50, ***$P < 0.0001$; control P50 versus Odd P50, ***$P < 0.0001$; one-way ANOVA with multiple comparisons for each area across age and unpaired *t* test to compare across exposure. In the boxplots, lines represent median, 25th, and 75th percentiles, + represents mean, whiskers represent 10th and 90th percentiles, and points below or above the whiskers are drawn as individual points.

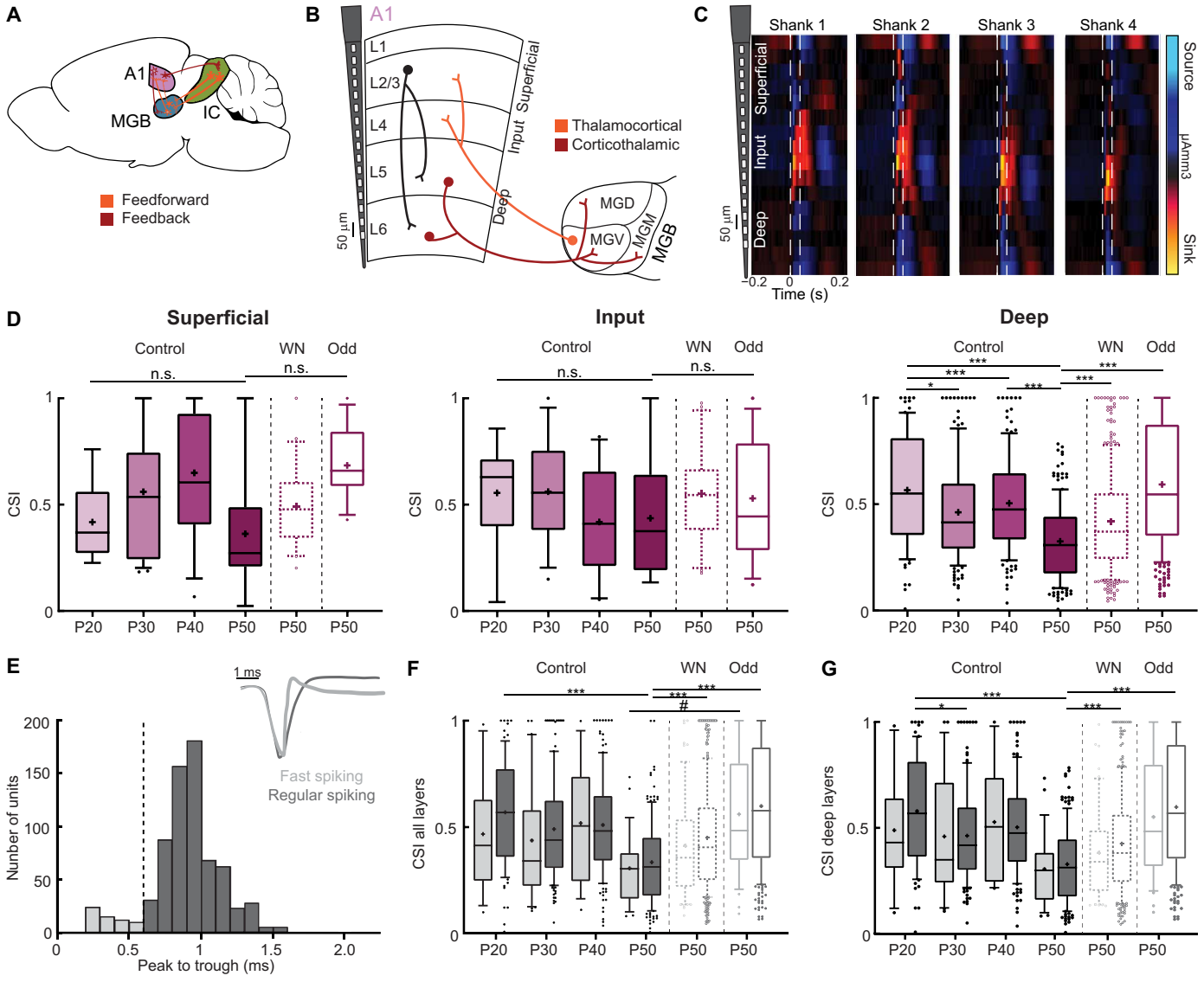

Fig. 5. A1 SSA maturation is specific to deep layers but not to cell type. (**A**) Schematic of mouse brain connectivity. (**B**) Schematic of A1 layer organization (L1/L2/3, superficial; L4, input; L5/L6, deep) and representative electrode shaft. Simplified A1 intracortical (black), thalamocortical (orange), and corticothalamic (brown) projections. (**C**) Example of CSD analysis (traced vertical lines, sound duration). (**D**) CSI for superficial (control: P20, 7 mice, 6 units; P30, 6 mice, 23 units; P40, 5 mice, 12 units; P50, 7 mice, 7 units; WN: P50, 7 mice, 20 units; Odd: P50, 4,11; $f = 2.29$, df = 78), input (control: P20, 9 units; P30, 12 units; P40, 10 units; P50, 6 units; WN: P50, 20 units; Odd: P50, 13 units; $f = 0.68$, df = 64), and deep (control: P20, 81 units; P30, 148 units; P40, 132 units; P50, 170 units; WN: P50, 325 units; Odd: P50, 282 units; $f = 32.29$, df = 1137) layers. n.s., $P > 0.05$; $^*P = 0.0120$; $^{***}P < 0.0001$. (**E**) Histogram of spike peak-to-trough duration (in milliseconds) for FS and RS units (dashed black line, threshold for classification). Inset: Example waveforms of FS and RS units. (**F**) CSI of FS and RS units for all layers [control: P20, 8 mice, 12 FS units, 84 RS units; P30, 6 mice, 30 FS units, 153 RS units; P40, 5 mice, 14 FS units, 140 RS units; P50, 7 mice, 27 FS units, 156 RS units; WN: P50, 7 mice, 69 FS units, 379 RS units; Odd: P50, 4 mice, 39 FS units, 267 RS units]. $^{***}P < 0.0001$; $^{\#}P = 0.06$. (**G**) CSI of FS and RS neurons for deep layers [control: P20, 11 FS units, 70 RS units; P30, 27 FS units, 121 RS units; P40, 10 FS units, 122 RS units; P50, 26 FS units, 144 RS units; WN: P50, 50 FS units, 275 RS units; Odd: P50, 35 FS units, 247 RS units; $f = 2.21$, df = 398]. $^*P = 0.0023$; $^{***}P < 0.0001$, one-way ANOVA with multiple comparisons for each area across age and unpaired *t* test to compare across exposure. In the boxplots, lines represent median, 25th, and 75th percentiles, + represents mean, whiskers represent 10th and 90th percentiles, and points below or above the whiskers are drawn as individual points.

responses to the oddball sequences (Fig. 6A). The experiment involved several steps: First, recordings were performed in A1 to identify its proper location and to calibrate the laser light power for correct A1 inactivation (fig. S6, A and B); then, the electrode was removed from A1 and inserted into MGV for the recording of neuronal responses to our oddball paradigm under light on (neuronal inhibition) or light off (control) conditions (see Materials and Methods). We verified that the CSI values in the MGV were not different between wild-type and PV-ChR2 mice without light stimulation (fig. S6D). For the light on condition, the laser was kept constantly on during each sequence length (400 ms to 3.55 s), shut off 50 ms after the end of the deviant tone, and turned on again when the next standard tone was played (250-ms light

off; Fig. 6B). We calculated the CSI and compared the light on and light off (control) conditions. For all age groups, CSI in MGV was significantly reduced upon optogenetic inhibition of A1 (Fig. 6C). When comparing CSI for all ages for the light on condition, we no longer observe a significant decrease at P30, P40, or P50 compared to the P20 group (Fig. 6D), indicating that the SSA changes observed in MGV are mainly due to corticofugal projections.

By light-activating PV cells across all cortical layers, we are not only inhibiting the corticothalamic projections but also inhibiting all projections from A1. These corticofugal projections also spread to the IC (*23*, *24*). To understand whether optogenetic manipulation of A1 affects only MGV or also ICC, we asked whether the same results would be observed in this area. We applied a similar optogenetic approach as for MGV but coupled it with ICC recordings (Fig. 6E). We did not observe any effect of A1 manipulation in ICC SSA at P40 when comparing the light off and light on conditions (Fig. 6F).

We then asked whether similar results would be observed if we specifically silenced corticothalamic projections from A1 L6 to MGV. These projections constitute one of the largest feedback pathways in the auditory system (*26*, *41*). To do so, we used a neurotensin receptor 1 (Ntsr1)–archaerhodopsin-3 (Arch) mouse line. Ntsr1-expressing neurons are one of the two major excitatory neuronal populations in cortical L6 (*42*–*44*). By crossing an Ntsr1-Cre line with an LoxP-Arch one, we obtained a specific expression of Arch in L6, which allowed light-induced inhibition of Ntsr1-expressing neurons and, consequently, of corticothalamic projections (see Materials and Methods). We anatomically confirmed Arch expression in Ntsr1 neurons in L6 (see Materials and Methods and fig. S6C). By coupling optogenetics with electrophysiology, we observed a significant CSI decrease in inhibition of corticothalamic projections, supporting the results obtained for the PV-ChR2 mice (Fig. 6, G and H).

Together, our results show that corticothalamic projections are implicated in the changes in SSA in MGV during adolescence. Although not significant, we observe an increasing effect of corticothalamic projections in regulating MGV SSA during this developmental period (ΔCSI means ± SEM in Fig. 6C, P20 = 0.127 ± 0.039, P30 = 0.132 ± 0.029, P40 = 0.146 ± 0.038, and P50 = 0.157 ± 0.043), which indicates that these circuits are still refining during adolescence. On the contrary, the corticocollicular projections appear stable during adolescence.

Last, we asked whether a perceptual correlate to the surprise response observed at the neuronal level could be identified. We video-monitored the mice during passive exposure to the oddball paradigm and analyzed the size of the pupil and the movement of the snout and ear using DeepLabCut (see Materials and Methods). Pupil size and snout movements did not change following standard or deviant sound stimuli. However, we were able to identify an ear movement associated with the sound presentation, but this response was the same for deviant and standard tones and did not differ across ages (fig. S7), suggesting that the response to the deviant is more than a reflex-like response and could not be tracked, with our approach, at the perceptual level in passively exposed mice.

DISCUSSION

Our study unravels how SSA matures in the central auditory system of adolescent mice and which neuronal circuits might underlie this

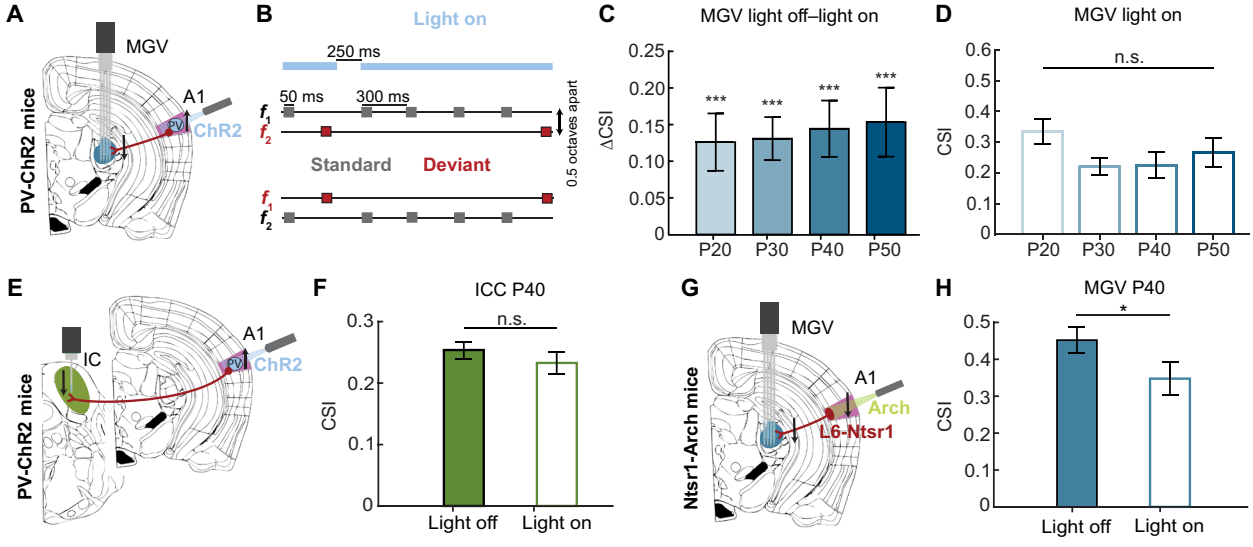

Fig. 6. Corticothalamic projections are implicated in SSA maturation. (**A**) Schematic of coronal slice including MGV (blue) and A1 (pink) location, light activation of PV-expressing ChR2 units, silencing of A1 corticofugal projections (brown), and parallel recordings in MGV. (**B**) Example schematic of light on condition for 2 of the 10 total oddball sequences. Light (473 nm) constantly on (blue) for the length of each sequence, turned off 50 ms after Deviant tone offset, and turned back on after 250 ms for the onset of standard tone. (**C**) Average CSI of light off–light on for MGV P20, P30, P40, and P50 (P20: 7 mice, 101 units; P30: 7 mice, 142 units; P40: 6 mice, 80 units; P50: 5 mice, 105 units). P20, $P = 0.0001$; P30, $P < 0.0001$; P40, $P = 0.0003$; P50, $P = 0.0004$; parametric paired *t* test light off versus light on per age. ***$P < 0.001$ (**D**) Average CSI for light on condition. n.s., $P > 0.05$, $f = 1.60$, df = 424; one-way ANOVA with multiple comparisons. (**E**) Schematic of coronal slice including ICC (green) and A1 (pink) location, light activation of PV-expressing ChR2 cells, silencing of A1 corticofugal projections (brown), and parallel recordings in IC. (**F**) Average CSI of light off–light on for ICC P40 (6 mice, 163 units). n.s, $P > 0.05$, parametric paired *t* test light off versus light on. (**G**) Schematic of coronal slice including MGV (blue) and A1 (pink) location, light (589 nm; green) inhibition of L6 Ntsr1-expressing cells projecting to MGV (brown), and parallel recordings in this area. (**H**) Averaged CSI spike rate of light off–light on for MGV P40 (5 mice, 71 units). Parametric paired *t* test light off versus light on; *$P < 0.05$. The bar graphs represent means ± SEM.

process. We first found the maturation of SSA across the lemniscal pathway of the central auditory system to be sequential. Although already stable at P20 in ICC, SSA develops until P30 in MGV and later in A1. We then observed that these changes do not only depend on the adaptation of the responses to the standard tone, suggesting a prominent role for PE or true deviance detection in this maturation. SSA maturation was also found to be independent of spontaneous activity, bandwidth, or threshold changes during adolescence. In addition, we identified A1 but not MGV SSA maturation to depend on prior sensory experience. Last, we observed A1 changes in deep but not input layers and MGV maturation to be regulated by corticothalamic projections.

We describe SSA processes during the maturation of the mouse auditory system rather than only in adulthood (*5*, *6*, *10*). We highlight the importance of the adolescent period for the refinement of sensory processing. Contrary to embryonic and early developmental stages (*45*–*48*), the degree of changes in the auditory system throughout adolescence is still not fully understood. In A1, the critical period for pure tones happens earlier that the juvenile time window studied here (P12 to P15 in mice) (*45*). However, a critical period for complex sounds was recently identified during the juvenile phase of mouse A1 development (P31 to P38) (*37*, *49*). This work raised the question of what other maturation processes might occur during this developmental phase (*50*). We consequently found SSA to still be maturing during mouse adolescence. These changes were not only unique to A1 but were also observed in the MGV (Fig. 7). We also report, in agreement with previous studies, a hierarchical SSA sensitivity along the central auditory pathway, from ICC to A1 (*1*, *5*). Unexpectedly, we found that SSA decreases with brain maturation. One possible explanation for this decrease is that listening strategies change with age. It has indeed been previously demonstrated that adults listen selectively for an expected test tone frequency, resulting in poor detection of low-probability tones. In contrast, infants listen more broadly and detect better than adults low probability tones (*51*). This observation would be compatible with a decrease in SSA with brain maturation. Additional experiments should be performed to test this speculation, for example, by measuring SSA across development in anesthetized animals.

Our study also puts forward a possible prominent role for other mechanisms than repetition suppression such as PE in the maturation of SSA (*1*, *5*, *6*, *52*, *53*). This idea of prediction, where the brain uses an internal model to predict sensory inputs based on previous experience, has been discussed through several lenses and sensory systems in the past (*53*–*57*). From an auditory perspective, PE defines an enhanced response to an unexpected sound that breaks the regularity encoded by a repetitive one. This violation is encoded as an error and sent to the higher levels of the auditory system (bottom-up pathway), causing an update in the representation of the corresponding stimuli and then a feedback signal predicting the error to the lower levels of the cascade (top-down pathway). The reduction and ablation of the PE are achieved through recurrent levels of bottom-up and top-down interactions (*5*, *58*).

PE neurons have been shown to exist across the different cortical layers and might even be enriched in the deep layers, where the main source of feedback signals is found (*53*, *59*–*61*). Our study shows evidence of top-down projections implicated in SSA. First, by studying SSA across A1 layers, we could identify intracortical maturation changes during adolescence. We did not observe any significant alterations in the input layer—the thalamocortical-recipient layer—which indicates that these feedforward projections are stable throughout adolescence. However, we identified changes in A1 deep layers, which include the corticofugal projections (Fig. 5). We

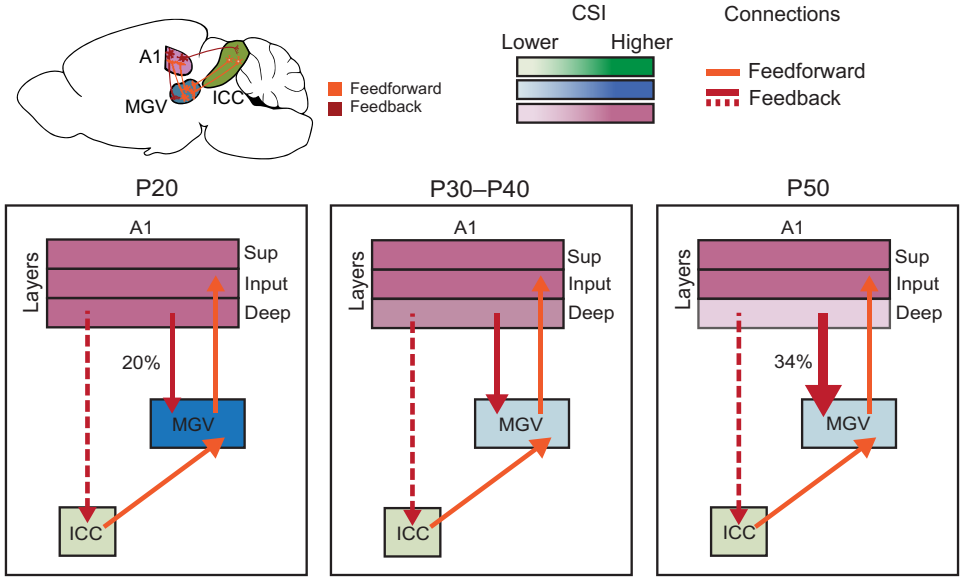

Fig. 7. Sequential maturation of SSA in the central auditory areas of adolescent mice. Schematic of connectivity organization and strength between the central auditory areas—ICC, MGV, and A1—during the adolescent period of mouse development. Color code: ICC, green; MGV, blue; A1, pink. Gradient of MGV and A1 color code: darker to lighter color, higher to lower CSI. Our data suggest that the feedforward connectivity (orange arrows) from ICC to MGV and from MGV to A1 and feedback connectivity (dashed red arrows) from A1 to ICC do not change significantly during adolescence. CSI of A1 deep layers decreases at P50. CSI in MGV decreases at P30. Feedback connectivity (red arrows) increase in strength throughout adolescence development with up-regulated percentage of CSI reduction in MGV with A1 silencing (20 to 34%).

then optogenetically inhibited corticothalamic projections across adolescence and identified a later refinement of this feedback circuitry underlying the maturation of surprise effect in MGV. These results further support the prior evidence of the role of these projections in regulating SSA in adult animals (*4*, *28*–*30*). They also point to a previous hypothesis that ascending auditory pathways mature first and their descending counterpart refines later in postnatal development (*62*). The authors of this study report the absent maturation of corticofugal projections before mouse hearing onset (P10 to P12) and discuss the advantage of delaying the refinement of projections responsible for feedback control until the feedforward pathways stabilize. In our study, the reduction of MGV CSI upon light activation goes from about 20% [0.13 (ΔCSI in MGV)/0.64 (CSI in A1) of PV-ChR2 mice; fig. S6E] at P20 to about 34% [0.16 (ΔCSI in MGV)/0.47 (CSI in A1) of PV-ChR2 mice; fig. S6E] of A1 CSI at P50 (Fig. 7). Furthermore, we identified the specific role of corticothalamic projections included in this reduction. Unlike the previous study (*29*), reducing cortical activity did not impose a change in CSI in the ICC. This mismatch might be due to methodological differences (cooling versus optogenetic silencing of cortex) or recording regions (nonlemniscal regions of IC in anesthetized rats versus ICC in awake mice).

PE circuits can also be shaped by experience, as previously shown in the primary visual cortex (*55*, *63*). Our study found A1 SSA maturation to depend on auditory experience during mouse adolescence. Both sensory masking of surprising sounds and overexposure to these stimuli caused CSI to be significantly larger than in control P50. Depriving the auditory neurons of deviant sounds during adolescence using continuous WN could alter the maturation process in A1, and the mice would remained strongly sensitive to surprise in adulthood. The opposite did not occur when mice were overexposed to the oddball paradigm. One possible interpretation of these results is that neurons become "experts" in deviance detection and consequently increase their response to the deviant instead of developing an expectation or adaptation for rare sounds and decreasing the surprise response. Another possibility is that overexposure to an oddball paradigm leads to increased anxiety, which, in turn, could increase response to deviant sounds. However, no signs of increased anxiety were observed in the exposed mice. What could then be the underlying factors causing these alterations in maturation? We found changes to occur at the level of deep layers of A1. However, so far, we did not find an obvious change in the contribution of excitatory versus inhibitory neurons, although interneurons have been shown to contribute in a specific way to SSA (*64*). Future studies should investigate possible mechanisms underlying this altered maturation upon changes in experience.

Our data also showed that changes in functional properties of the cells did not correlate with CSI. It was previously shown that FRA properties of the auditory neurons correlate with specific levels of SSA (*16*, *17*). Higher CSI levels were related to higher frequencies played at low intensities and broader bandwidth of the tuning curve. However, we did not find a significant correlation between the observed deviant changes with bandwidth or threshold. The seemingly contradictory observations might be related to different factors, particularly the developmental focus followed in our study.

This study also raises other follow-up questions. One of them relies on possible other areas implicated in the regulation of surprising sound processing. In addition to the nonlemnical pathway that surely plays an important role in coding for SSA, one could examine whether the thalamic reticular nuclei (TRN), which also receives Ntsr1-expressing neurons inputs (*43*), is involved in the changes we observe for SSA in MGV. By silencing these L6 corticothalamic projections, we might be affecting the inhibitory role of TRN over MGB and contributing to the outcome we observe when silencing A1. Because of known cross-talk between the auditory areas with other brain regions, the observed changes in the A1 surprise effect might also depend on the circuits established with other regions. Besides other auditory nuclei, the corticofugal projections spread to the visual cortex or prefrontal cortex (PFC), among other areas (*52*, *65*). In humans, SSA was argued to be mediated by input from the PFC (*66*). More recently, a study recorded responses in rats' middle PFC to the oddball paradigm and identified PE to drive auditory responsiveness in this area (*52*). PE should also be further explored in the developing central auditory areas. Another protocol used as control, combining the many-standard and cascade sequences, could be coupled to the oddball paradigm to understand better how PE occurs along the developing auditory pathways. The many-standard sequence corresponds to a random presentation of 10 selected pure tones with different frequencies played the same number of times. The cascaded sequence contains the same 10 tones but arranged in an ascending or descending frequency order (*5*, *30*, *67*). Last, more could be inferred about the experience-dependent plasticity of SSA through, for example, auditory perceptual tasks, such as detection task, with standard and deviant as stimuli, and compare the performance of WN and oddball-exposed versus control mice (*68*). We could also explore the cortical synapses that might undergo these plastic changes using optogenetics or chemogenetics and activate or inhibit a particular neuronal population to assess how it affects the perceptual learning of the mice.

Most of the reported auditory developmental knowledge was acquired in animals. However, it has a high potential for translational application in humans, as the maturation of auditory skills in humans very much parallels the one in mice (*45*, *49*, *69*–*73*). The knowledge provided in this work improves our understanding of how the response to surprising sounds is appropriately fitted to the environment in which a plastic brain matures, especially a still vulnerable adolescent brain. Ultimately, ours and other studies on developmental plasticity will help us understand when the brain is plastic, what controls this plasticity, and which neural networks are engaged for different sensory stimuli.

MATERIALS AND METHODS

Animals

All experimental procedures were performed by following Basel University animal care and use guidelines, approved by the Veterinary Office of the Canton Basel-Stadt, Switzerland. C57BL/6J mice (SC-C57J-M, Janvier, France) were aged 19 days (P19) to 8 weeks old, and males and females were used without distinction. PV-ChR2 mice were derived from crossing a PV-Cre knock-in line with C57BL/6J background (JAX stock number 017320, the Jackson laboratories, ME, USA) with a ChR2-floxed Ai32 line (JAX stock number 024109, C57BL/6J background). The animals were aged P19 to 8 weeks old. Ntsr1-Arch mice were derived from crossing an Ntsr1-Cre knock-in line with C57BL/6J background [Mutant Mouse Resource and Research Center (MMRRC) stock number 030648-UCD] with an Arch-floxed Ai32 line (JAX stock number 012735, the Jackson laboratories, ME, USA). These animals were aged P38 to P42 days. After weaning, mice were housed

in groups of two to five under a 12-hour light/12-hour dark cycle and allowed to get food and water ad libitum. Experiments were performed in the light phase.

Surgical procedures

Mice were anesthetized with isoflurane in O_2 (4% induction and 1.2 to 2.5% maintenance), and local analgesia was provided with subcutaneous injection of bupivacaine/lidocaine (0.01 and 0.04 mg per animal, respectively). The depth of anesthesia was monitored by the breathing rate and absence of pinch withdrawal reflex. Body temperature was maintained at 37°C via a heating pad (FHC, ME, USA), and lubricant ophthalmic ointment was applied on both eyes. A custom-made stainless steel head-restraint post was fixed on the bone on top of the left hemisphere and used to head-fix the animals. By using a scalpel, a craniotomy (~2 mm by 2 mm) was performed just above the ICC, MGV, or the ACx. The dura was left intact and was covered with silicone oil to prevent drying. The craniotomy was covered with a thick layer of Kwik-Cast sealant (World Precision Insturments, Sarasota, FL, USA) to protect it from external agents. Mice were placed back in their home cage for 2 hours to recover from anesthesia.

Awake electrophysiological recordings

After a 2-hour recovery period, the craniotomy was exposed and covered with silicon oil. A 1 × 32 electrode (A1×32-5 mm-25-177-A32, Neuronexus, MI, USA) was inserted in ICC with a motorized stereotaxic micromanipulator (DMA-1511, Narishige, Japan) at depths of (tip of electrode) 800 ± 100 and 1400 ± 100 μm from pia. Recordings from the ICC were confirmed in each penetration by increasing averaged BF from the most dorsal to the most ventral channels, confirming the tonotopic organization typical of IC. A 4 × 16 electrode (A4×16-3 mm-50-200-177-A64, Neuronexus, MI, USA) was inserted in A1 at a depth of 950 ± 50 μm from pia, traversing the superficial, input, and deep layers. Recordings from A1 were confirmed in each penetration by increasing averaged BF from the most caudal to the most rostral shaft of the four-shaft electrodes, confirming the tonotopic organization typical of A1. A 4 × 16 electrode (A4×16-5 mm-50-200-177-A64, Neuronexus, MI, USA) was inserted in MGV at a depth of 3500 ± 100 μm from pia. Recordings from MGV were confirmed in each penetration based on auditory responses along the four-shaft electrode. All recordings were performed in a sound-attenuating chamber (modified MAC-2 chambers, Industrial Acoustics Company Nordics, Hvidorve, Denmark). At the end of the recording session, each mouse was euthanized with an intraperitoneal injection of pentobarbital followed by cervical dislocation.

Auditory stimulations

Sounds were generated with a digital signal processor (RZ6, Tucker Davis Technologies, FL, USA; 200-kHz sampling rate) and played through an electrostatic speaker (ES1, Tucker Davis Technologies, FL, USA) positioned at 5 to 7 cm from the mouse's left ear. Stimuli were calibrated with a wide-band ultrasonic acoustic sensor (model 378C01, PCB Piezotronics, NY, USA). For the organization of FRAs, pure frequency tones (50-ms duration and 4-ms cosine on/off ramps) from 4 to 64 kHz in 0.1-octave increments and 0- to 80-dB SPL in 5-dB increments were played with randomized interstimulus intervals (ISIs) of 500 to 1000 ms and repeated twice. This protocol allowed the examination and confirmation of tonotopy for each area, as well as the selection of the two frequencies for the oddball sequence paradigm (standard and deviant tones). The channel with the largest responses was selected, and two frequencies on either side of the BF of that channel were chosen. The lower frequency was denoted f_1, the higher frequency was denoted f_2, and they were selected such that $f_2/f_1 = 1.5$, corresponding to an interval of 0.5 octaves. We tested the responses to these frequencies in sets of 10 different sequences, with 1 to 10 standards preceding a deviant tone (50-ms duration, 4-ms cosine on/off ramps, and 65-dB SPL). The sequences were randomly assigned and repeated 15 times with an ISI (offset of tone to onset of next one) of 300 ms, both within and between sequences. These sequences yielded a probability of occurrence of ~85 and 15% of standard and deviant, respectively. This paradigm was presented two times. For the second time, f_1 and f_2 frequencies were swapped to inspect a response dependency to the different frequencies used. Our protocol was based on previous studies (*12*, *18*). For the laser calibration, 50-ms pure tones (4-ms cosine on/off ramps and 500-ms ISI) were coupled to 400-ms on/off light stimuli (0.01-ms cosine on/off ramps). For the silencing of A1, the oddball sequence paradigm was coupled with the laser. A blue or green laser was kept constantly on for the length of each sequence (400 ms to 3.55 s). Shutting off the laser was delayed 50 ms after deviant tone termination and lasted for 250 ms. For the identification of the cortical layers, we delivered 50-ms bursts of broadband noise (4-ms cosine on/off ramps and 500-ms ISI).

Optogenetic manipulation

Optogenetic was coupled to the awake electrophysiological recordings. Two craniotomies (~2 mm by 2 mm) were performed just above the MGB or IC and the ACx and covered with silicon oil and Kwik-Cast sealant. Mice were placed back in their home cage for 2 hours to recover from anesthesia. After this period, the craniotomies were exposed and covered with silicon oil. A 4 × 16 electrode (A4×16-3 mm-50-200-177-A64, Neuronexus, MI, USA) was used to identify the A1 location (confirmed by tonotopy). A blue (ChR2) or green (Arch) laser (473 and 589 nm, respectively) was placed close to the four-shaft electrode and above A1. The laser light was calibrated before experiments. The blue laser was applied to the cortical surface to activate PV-expressing neurons and consequently silence cortical excitatory neurons (*74*). The green laser was used to inhibit L6 corticothalamic neurons (*26*). The power was calibrated for each mouse recorded and set between 2 and 5 mW. The electrode was then removed from A1 without moving the laser. A 4 × 16 (A4×16-5 mm-50-200-177-A64, Neuronexus, MI, USA) or 1 × 32 electrode (A1×32-5 mm-25-177-A32, Neuronexus, MI, USA) was inserted into MGV or ICC, respectively, with a motorized stereotaxic micromanipulator (DMA-1511, Narishige, Japan) at a depth of 3500 ± 100 μm or 800 and 1400 ± 100 μm from pia, respectively. The oddball sequence paradigm was recorded with and without blue light as control versus silencing of A1. For A1 L6 corticothalamic neuron inhibition, a 4 × 16 (A4×16-5 mm-50-200-177-A64, Neuronexus, MI, USA) was inserted into MGV. The oddball sequence paradigm was recorded with and without green light as control versus inhibition of corticothalamic projections.

Sound exposure

Mice were placed in a custom-made sound-attenuating chamber and exposed to continuous WN or oddball sequence paradigm from P20 to P50. WN (bandwidth from 1 to 65 kHz and 75-dB SPL played continuously for the whole exposure period) was generated by an

arbitrary function generator (model AFG1022, Tektronix, Beaverton, USA), amplified by an integrated amplifier (model PM7005, Marantz Kawasaki, Japan), and played through a magnetic speaker (MF1, Tucker Davis Technologies, FL, USA) positioned 35 cm above the bottom of the cage. The oddball used for the exposure was identical to the one of the recordings. Mice were exposed to fixed f_1 and f_2 frequencies (11 and 16.5 kHz played and chosen in accordance to best responses obtained previously in the recordings) at 65-dB SPL for 3 hours every day. Animals were kept for the rest of the time in housing cabinet. Animals were housed with same-gender littermates, had access to water and food ad libitum, and moved about freely in their cage. Awake electrophysiological recordings were performed after sound exposure in MGV or A1 while passively exposed to the oddball sequence paradigm.

Histology

For the study of the anatomical location of IC, MGB, and ACx penetrations, respective electrodes were brushed with a Dil dye (Thermo Fisher Scientific, V22885, USA) at the end of the electrophysiological recordings. The brushed electrode was inserted in identical coordinates and depth of recorded penetrations and left inside for 2 to 3 min before removal. Mice were then deeply anesthetized with an intraperitoneal injection of pentobarbital and transcardially perfused with saline, followed by 4% paraformaldehyde (PFA; 441244, Sigma-Aldrich, USA) in 0.1 M phosphate-buffered saline (PBS; P3813, Sigma-Aldrich) (pH 7.4) at 4°C. Brains were dissected and postfixed overnight in 4% PFA, cryoprotected with 30% sucrose for 2 days, embedded in dry-ice frozen optimal cutting temperature (OCT) compound (TissueTek, Sakura Finetek, Germany), and kept at −80°C. Coronal slices (45 μm) were prepared with a cryostat (CM3050 S, Leica, Germany). Slices were blocked in 0.05% Triton X-100 (X100, Sigma-Aldrich) in PBS (PBS-T) for 1 hour at room temperature (RT) and incubated overnight in 10% donkey serum (C06SBZ, Bio-Rad, USA) in PBS-T containing the primary antibodies. On the following day, a 2-hour incubation at RT was executed for immunoreaction with the secondary antibodies. All slices were counterstained with fluorescent 4,6-diamidino-2-phenylindole, dihydrochloride (D1306, Thermo Fisher Scientific) to stain for cell nuclei and mounted with Fluoromount-G (0100–01, SouthernBiotech, USA). For the MGB brain slices, immunostaining for calretinin cells was performed to identify its divisions (calretinin-expressing not found in MGV but dorsal and middle MGB) (*75*). For the IC brain slices, immunostaining for the glycine 2 transporter was performed to identify its divisions (glycine 2 is abundant in ICC) (*76*). To confirm Arch expression in L6 Ntsr1 neurons, an antibody was used against green fluorescent protein (GFP) endogenous in the mouse line. The following primary antibodies were used: goat anti-calretinin (CG1, Swant, Switzerland; 1:1000), rabbit anti–glycine 2 (273003, Synaptic Systems, Germany; 1:500), and chicken anti-GFP (GFP-1020, Aves Labs Inc., USA; 1:1000), respectively. For secondary antibodies, we used the following: donkey anti-goat Alexa Fluor 488 (A-11055, Thermo Fisher Scientific; 1:1000), donkey anti-rabbit Alexa Fluor 488 (A-21206, Thermo Fisher Scientific; 1:500), and donkey anti-chicken Alexa Fluor 488 (703-545-155, Jackson ImmunoResearch, 1:1000), respectively.

Body movement tracking

Mice were video monitored with a high-resolution infrared-sensitive camera (BFS-U3-16S2M-CS, FLIR Systems) focused on the face contralateral to the recording site through a zoom lens (TCL 1216 5MP, ImagingSource, Charlotte, NC, USA). Bright uniform illumination of the eye was achieved using two red light-emitting diode lights (50668 Micro Light LED, Büchel). Frame acquisition was triggered at 30 Hz by a transistor-transistor logic (TTL) pulse sent by the system also delivering sounds (RZ6, Tucker Davis Technologies, FL, USA). Storage of TTL time stamps allowed for post hoc synchronization of video frames, sound stimulation, and neural recordings. The pupil size, ear, and snout movements were tracked using the deep learning software package DeepLabCut (*77*). The experimenter manually labeled the top, right, bottom, and left borders of the mouse's pupil and ear in 20 frames extracted for five animals per age group, which were then used to train the network. On the basis of manual inspection of the extracted positions' accuracy, only extracted data with a confidence level higher than 0.85 were kept. Missing data were filled using linear interpolation.

Data processing

Responses from extracellular recordings were digitized with a 64-channel recording system (RZ2 BioAmp processor, Tucker Davis Technologies, FL, USA) at 24,414 Hz. Putative single and multiunits were identified offline using KiloSort (CortexLab, UCL, London, England) (*78*), followed by manual inspection of spike shape and signal-to-noise ratio and auto- and cross-correlograms using Phy (CortexLab, UCL, London, England). Both single- and multiunits were retained for analysis. Here, "unit" refers to both single and multiunits as an approximation of a single neuron. Further analysis was performed using custom software in MATLAB (MathWorks, MA, USA).

Data analysis

FRAs were calculated in a fixed time window from tone onset (0 to 60 ms), smoothed with a median filter (4 × 4 sampling window), and thresholded to 20% of maximal response amplitude. This threshold was implemented only to determine the boundary of the FRAs (all other data analysis was performed on the raw, nonthresholded data). To assess the tuning quality of the FRA, d' was calculated as the difference in mean spike count within the FRA and mean spike count outside the boundary of FRA divided by their arithmetic average SD [modified method from (*49*)]. For the analysis, units with $d' > 0.5$, BF between 4 and 64 kHz, onset latency of <15 (ICC), <30 (MGV), and <35 (A1) ms, and threshold of <70-dB SPL were selected. BF was defined as the tone frequency that evoked the highest response at all tested sound levels. A1 and ICC were identified on the basis of the functional tonotopy (caudorostral and dorsoventral increase in BF, respectively) and MGV by the presence of auditory responses. Data that could not be identified as belonging to ICC, MGV, or A1 were excluded from the analysis. For the analysis of responses to the oddball sequence paradigm, units with significant responses to only standard or deviant tone, or to both tones, were selected. Responses were also analyzed in a fixed time window from tone onset (0 to 60 ms). Mean spike rates were used to calculate the SI and CSI. SI was determined by calculating the difference between the average firing rates in a window of 0 to 60 ms from tone onset to the standard and deviant tones for f_1 or f_2 (SI f_1 and SI f_2)

$$\mathrm{SI} = \frac{\mathrm{DT}(f_i) - \mathrm{ST}(f)}{\mathrm{DT}(f_i) + \mathrm{ST}(f)}$$

CSI was calculated by combining SI f_1 and SI f_2 calculations

$$\mathrm{CSI} = \frac{\mathrm{DT}(f_i) + \mathrm{ST}(f_2) - \mathrm{ST}(f_1) - \mathrm{ST}(f_2)}{\mathrm{DT}(f_i) + \mathrm{ST}(f_2) + \mathrm{ST}(f_1) + \mathrm{ST}(f_2)}$$

Two analyses were performed: (i) SI and CSI calculation of the average of each 15-repeated sequence and average of the 10 sequences and (ii) SI and CSI calculation for the first standard in each sequence in comparison to deviant tone of corresponding frequency (f_1 or f_2). For the (ii), we applied a different analytical approach. We calculated the CSI for each sequence (1 to 10 standards preceding a deviant). To do so, we averaged the spike response rate to the deviant tone and compared it to the response to the first standard in each sequence of the same frequency (f_1 or f_2) (fig. S3D). Our approach differs from previous studies, where the authors only looked at the last standard for each sequence to do this analysis (*79*).

For the adaptation analysis (fig. S4), we fitted the average firing rate of the responses to the standard or the deviant normalized to the first sound stimulus (standard or deviant, respectively) over the first 75 or 25 sounds, respectively, with the exponential function $(1-a) \times \exp(-t/\text{tau}) + a$. To evaluate the variability of the fits, the average firing rates were the results of 1000 iterations of 80% of the data using the MATLAB function "datasample." The fit functions in fig. S4A are the exponential functions obtained with the average a and tau values over the 1000 iterations for each age and area. The parameters a and tau represented in fig. S4 (C and D) are the distribution of the values obtained in the 1000 iterations.

We also normalized standard and deviant tone response for each sequence by dividing spike rate of tones position in the sequence (1 to 9 for standard and 2 to 10 for deviant) to the sequence with a single standard (0 position for standard and 1 for deviant). The normalization was further applied on the total number of trials (975) in the oddball protocol for standard (825) and deviant (150).

For the identification of the cortical layers (A1), CSD analysis of local field potentials (LFPs) was performed. We extracted LFP by downsampling the raw voltage traces to 1 kHz and low-pass filtering (<300 Hz) with an eighth-order Chebyshev type I filter. We then performed CSD analysis on the data from each electrode shank as described in Pettersen *et al.* (*80*), using an adapted version of the CSD_plotter toolbox function "my_standardCSD" (https://github.com/espenhgn/CSDplotter). CSD was performed for each electrode shaft by calculating the second spatial derivative of the LFPs across the depth of A1 (Fig. 5C). We measured the current amplitude for the sink (input) and source (output) layers. Electrode channels located in input layers were then manually identified as the ones belonging to the largest short onset current sink (*38*, *43*, *59*). Channels located above the deepest sink were classified as located in superficial layers and those below as located in deep layers. Each unit was classified as belonging to superficial, input, or deep layers based on the channel in which its spike amplitude was the largest.

For the classification of A1 populations, cortical units were classified as RS (putative excitatory neurons) or FS (putative PV-expressing neurons) by extracting the peak to trough of the average spike shape for each unit. On the basis of the bimodal distribution of this parameter across the population, we defined units with a peak to trough of <0.6 ms as FS and ≥0.6 as RS (*39*, *40*).

Statistical analysis

Statistical tests were performed using MATLAB (MathWorks, MA, USA) and GraphPad Prism software (GraphPad Software, USA). In the boxplots, lines represent median, 25th, and 75th percentiles, + represents mean, whiskers represent 10th and 90th percentiles, and points below or above the whiskers are drawn as individual points. A one-way analysis of variance (ANOVA) with Holm-Sidak's multiple comparisons test was used to calculate whether there were differences across ages among the different areas for CSI and functional properties in control and exposed mice (Figs. 1, F to I; 3, A, C, and E; 4, C, E, and H; 5, D, F, and G; and 6D; and figs. S2, C and D, and S4E) and a Kruskal-Wallis to compare the parameters of the exponential fits (fig. S4, C and D). An unpaired Student's *t* test was used to compare functional properties between control and exposed mice (Fig. 4, C, E, and H, and figs. S5 and S6, D and E). A paired Student's *t* test was used to calculate whether there was an effect of light on versus light off conditions in the different optogenetic approaches (Fig. 6, C, F, and H, and fig. S6B). A Pearson correlation was performed, followed by a simple linear regression to assess possible relations between functional properties and experimental parameters with CSI across ages and areas (Fig. 3, B, D, and E, and fig. S5). For the video analysis (fig. S7), a Wilcoxon signed-rank test was used to compare pre- and poststimulus responses, and a Wilcoxon rank sum test was used to compare responses to standard and deviant tones.

Supplementary Materials

This PDF file includes:

Figs. S1 to S7
Table S1

REFERENCES AND NOTES

1. M. Font-Alaminos, T. Ribas-Prats, N. Gorina-Careta, C. Escera, Emergence of prediction error along the human auditory hierarchy. *Hear. Res.* **399**, 107954 (2021).
2. K. Kompus, R. Westerhausen, A. R. Craven, K. Kreegipuu, N. Põldver, S. Passow, K. Specht, K. Hugdahl, R. Näätänen, Resting-state glutamatergic neurotransmission is related to the peak latency of the auditory mismatch negativity (MMN) for duration deviants: An ^{1}H-MRS-EEG study. *Psychophysiology* **52**, 1131–1139 (2015).
3. R. Naatanen, P. Paavilainen, T. Rinne, K. Alho, The mismatch negativity (MMN) in basic research of central auditory processing: A review. *Clin. Neurophysiol.* **118**, 2544–2590 (2007).
4. P. Bauerle, W. von der Behrens, M. Kossl, B. H. Gaese, Stimulus-specific adaptation in the gerbil primary auditory thalamus is the result of a fast frequency-specific habituation and is regulated by the corticofugal system. *J. Neurosci.* **31**, 9708–9722 (2011).
5. G. G. Parras, J. Nieto-Diego, G. V. Carbajal, C. Valdés-Baizabal, C. Escera, M. S. Malmierca, Neurons along the auditory pathway exhibit a hierarchical organization of prediction error. *Nat. Commun.* **8**, 2148 (2017).
6. N. Taaseh, A. Yaron, I. Nelken, Stimulus-specific adaptation and deviance detection in the rat auditory cortex. *PLOS ONE* **6**, e23369 (2011).
7. L. A. Anderson, G. B. Christianson, J. F. Linden, Stimulus-specific adaptation occurs in the auditory thalamus. *J. Neurosci.* **29**, 7359–7363 (2009).
8. M. Dong, D. S. Vicario, Neural correlate of transition violation and deviance detection in the songbird auditory forebrain. *Front. Syst. Neurosci.* **12**, 46 (2018).
9. N. Ulanoversusky, L. Las, I. Nelken, Processing of low-probability sounds by cortical neurons. *Nat. Neurosci.* **6**, 391–398 (2003).
10. M. S. Malmierca, S. Cristaudo, D. Perez-Gonzalez, E. Covey, Stimulus-specific adaptation in the inferior colliculus of the anesthetized rat. *J. Neurosci.* **29**, 5483–5493 (2009).
11. Y. A. Ayala, D. Perez-Gonzalez, D. Duque, I. Nelken, M. S. Malmierca, Frequency discrimination and stimulus deviance in the inferior colliculus and cochlear nucleus. *Front. Neural. Circuits* **6**, 119 (2013).
12. F. M. Antunes, I. Nelken, E. Covey, M. S. Malmierca, Stimulus-specific adaptation in the auditory thalamus of the anesthetized rat. *PLOS ONE* **5**, e14071 (2010).
13. M. Harpaz, M. M. Jankowski, L. Khouri, I. Nelken, Emergence of abstract sound representations in the ascending auditory system. *Prog. Neurobiol.* **202**, 102049 (2021).
14. I. Hershenhoren, N. Taaseh, F. M. Antunes, I. Nelken, Intracellular correlates of stimulus-specific adaptation. *J. Neurosci.* **34**, 3303–3319 (2014).
15. Y. Y. Zhai, Z. H. Sun, Y. M. Gong, Y. Tang, X. Yu, Integrative stimulus-specific adaptation of the natural sounds in the auditory cortex of the awake rat. *Brain Struct. Funct.* **224**, 1753–1766 (2019).
16. D. Duque, D. Perez-Gonzalez, Y. A. Ayala, A. R. Palmer, M. S. Malmierca, Topographic distribution, frequency, and intensity dependence of stimulus-specific adaptation in the inferior colliculus of the rat. *J. Neurosci.* **32**, 17762–17774 (2012).

17. J. Nieto-Diego, M. S. Malmierca, Topographic distribution of stimulus-specific adaptation across auditory cortical fields in the anesthetized rat. *PLoS Biol.* **14**, e1002397 (2016).
18. A. Polterovich, M. M. Jankowski, I. Nelken, Deviance sensitivity in the auditory cortex of freely moving rats. *PLOS ONE* **13**, e0197678 (2018).
19. J. G. Mellott, N. L. Foster, A. P. Ohl, B. R. Schofield, Excitatory and inhibitory projections in parallel pathways from the inferior colliculus to the auditory thalamus. *Front. Neuroanat.* **8**, 124 (2014).
20. H. Redies, S. Brandner, O. D. Creutzfeldt, Anatomy of the auditory thalamocortical system of the guinea pig. *J. Comp. Neurol.* **282**, 489–511 (1989).
21. P. H. Smith, D. J. Uhlrich, K. A. Manning, M. I. Banks, Thalamocortical projections to rat auditory cortex from the ventral and dorsal divisions of the medial geniculate nucleus. *J. Comp. Neurol.* **520**, 34–51 (2012).
22. M. F. Happel, M. Jeschke, F. W. Ohl, Spectral integration in primary auditory cortex attributable to temporally precise convergence of thalamocortical and intracortical input. *J. Neurosci.* **30**, 11114–11127 (2010).
23. M. M. Asokan, R. S. Williamson, K. E. Hancock, D. B. Polley, Sensory overamplification in layer 5 auditory corticofugal projection neurons following cochlear nerve synaptic damage. *Nat. Commun.* **9**, 2468 (2018).
24. V. M. Bajo, F. R. Nodal, D. R. Moore, A. J. King, The descending corticocollicular pathway mediates learning-induced auditory plasticity. *Nat. Neurosci.* **13**, 253–260 (2010).
25. D. K. Ryugo, N. M. Weinberger, Corticofugal modulation of the medial geniculate body. *Exp. Neurol.* **51**, 377–391 (1976).
26. R. S. Williamson, D. B. Polley, Parallel pathways for sound processing and functional connectivity among layer 5 and 6 auditory corticofugal neurons. *eLife* **8**, (2019).
27. J. A. Winer, Decoding the auditory corticofugal systems. *Hear. Res.* **207**, 1–9 (2005).
28. F. M. Antunes, M. S. Malmierca, Effect of auditory cortex deactivation on stimulus-specific adaptation in the medial geniculate body. *J. Neurosci.* **31**, 17306–17316 (2011).
29. L. A. Anderson, M. S. Malmierca, The effect of auditory cortex deactivation on stimulus-specific adaptation in the inferior colliculus of the rat. *Eur. J. Neurosci.* **37**, 52–62 (2013).
30. A. M. H. Lesicko, C. F. Angeloni, J. M. Blackwell, M. De Biasi, M. N. Geffen, Corticofugal regulation of predictive coding. *Elife* **11**, e73289 (2022).
31. N. Ulanoversusky, L. Las, D. Farkas, I. Nelken, Multiple time scales of adaptation in auditory cortex neurons. *J. Neurosci.* **24**, 10440–10453 (2004).
32. I. Erchova, A. Vasalauskaite, V. Longo, F. Sengpiel, Enhancement of visual cortex plasticity by dark exposure. *Philos. Trans. R. Soc. Lond. B Biol. Sci.* **372**, 20160159 (2017).
33. N. Tian, C. Petersen, S. Kash, S. Baekkeskov, D. Copenhagen, R. Nicoll, The role of the synthetic enzyme GAD65 in the control of neuronal gamma-aminobutyric acid release. *Proc. Natl. Acad. Sci. U.S.A.* **96**, 12911–12916 (1999).
34. W. J. Speechley, J. L. Hogsden, H. C. Dringenberg, Continuous white noise exposure during and after auditory critical period differentially alters bidirectional thalamocortical plasticity in rat auditory cortex in vivo. *Eur. J. Neurosci.* **26**, 2576–2584 (2007).
35. C. Xia, M. Yin, P. Pan, F. Fang, Y. Zhou, Y. Ji, Long-term exposure to moderate noise induces neural plasticity in the infant rat primary auditory cortex. *Anim Cells Syst (Seoul)* **23**, 260–269 (2019).
36. J. Xu, L. Yu, R. Cai, J. Zhang, X. Sun, Early continuous white noise exposure alters auditory spatial sensitivity and expression of GAD65 and GABAA receptor subunits in rat auditory cortex. *Cereb. Cortex* **20**, 804–812 (2010).
37. M. Nakamura, P. Valerio, S. Bhumika, T. R. Barkat, Sequential organization of critical periods in the mouse auditory system. *Cell Rep.* **32**, 108070 (2020).
38. G. De Franceschi, T. R. Barkat, Task-induced modulations of neuronal activity along the auditory pathway. *Cell Rep.* **37**, 110115 (2021).
39. S. Q. Lima, T. Hromadka, P. Znamenskiy, A. M. Zador, PINP: A new method of tagging neuronal populations for identification during in vivo electrophysiological recording. *PLOS ONE* **4**, e6099 (2009).
40. L. G. Nowak, R. Azouz, M. V. Sanchez-Vives, C. M. Gray, D. A. McCormick, Electrophysiological classes of cat primary visual cortical neurons in vivo as revealed by quantitative analyses. *J. Neurophysiol.* **89**, 1541–1566 (2003).
41. J. J. Prieto, J. A. Winer, Layer VI in cat primary auditory cortex: Golgi study and sublaminar origins of projection neurons. *J. Comp. Neurol.* **404**, 332–358 (1999).
42. D. S. Bortone, S. R. Olsen, M. Scanziani, Translaminar inhibitory cells recruited by layer 6 corticothalamic neurons suppress visual cortex. *Neuron* **82**, 474–485 (2014).
43. W. Guo, A. R. Clause, A. Barth-Maron, D. B. Polley, A corticothalamic circuit for dynamic switching between feature detection and discrimination. *Neuron* **95**, 180–194.e5 (2017).
44. S. R. Olsen, D. S. Bortone, H. Adesnik, M. Scanziani, Gain control by layer six in cortical circuits of vision. *Nature* **483**, 47–52 (2012).
45. T. R. Barkat, D. B. Polley, T. K. Hensch, A critical period for auditory thalamocortical connectivity. *Nat. Neurosci.* **14**, 1189–1194 (2011).
46. R. Deng, J. P. Y. Kao, P. O. Kanold, Distinct translaminar glutamatergic circuits to GABAergic interneurons in the neonatal auditory cortex. *Cell Rep.* **19**, 1141–1150 (2017).
47. B. Gurung, B. Fritzsch, Time course of embryonic midbrain and thalamic auditory connection development in mice as revealed by carbocyanine dye tracing. *J. Comp. Neurol.* **479**, 309–327 (2004).
48. R. Romand, G. Ehret, Development of tonotopy in the inferior colliculus. I. Electrophysiological mapping in house mice. *Brain Res. Dev. Brain Res.* **54**, 221–234 (1990).
49. S. Bhumika, M. Nakamura, P. Valerio, M. Solyga, H. Lindén, T. R. Barkat, A late critical period for frequency modulated sweeps in the mouse auditory system. *Cereb. Cortex* **30**, 2586–2599 (2020).
50. S. Vinogradov, M. V. Chafee, E. Lee, H. Morishita, Psychosis spectrum illnesses as disorders of prefrontal critical period plasticity. *Neuropsychopharmacology* **48**, 168–185 (2023).
51. J. Y. Bargones, L. A. Werner, Adults listen selectively - Infants do not. *Psychol. Sci.* **5**, 170–174 (1994).
52. L. Casado-Roman, G. V. Carbajal, D. Perez-Gonzalez, M. S. Malmierca, Prediction error signaling explains neuronal mismatch responses in the medial prefrontal cortex. *PLoS Biol.* **18**, e3001019 (2020).
53. G. B. Keller, T. Bonhoeffer, M. Hubener, Sensorimotor mismatch signals in primary visual cortex of the behaving mouse. *Neuron* **74**, 809–815 (2012).
54. S. J. Eliades, X. Wang, Neural substrates of vocalization feedback monitoring in primate auditory cortex. *Nature* **453**, 1102–1106 (2008).
55. A. Fiser, D. Mahringer, H. K. Oyibo, A. V. Petersen, M. Leinweber, G. B. Keller, Experience-dependent spatial expectations in mouse visual cortex. *Nat. Neurosci.* **19**, 1658–1664 (2016).
56. G. B. Keller, R. H. Hahnloser, Neural processing of auditory feedback during vocal practice in a songbird. *Nature* **457**, 187–190 (2009).
57. R. P. Rao, D. H. Ballard, Predictive coding in the visual cortex: A functional interpretation of some extra-classical receptive-field effects. *Nat. Neurosci.* **2**, 79–87 (1999).
58. M. Mittag, R. Takegata, I. Winkler, Transitional probabilities are prioritized over stimulus/pattern probabilities in auditory deviance detection: Memory basis for predictive sound processing. *J. Neurosci.* **36**, 9572–9579 (2016).
59. A. M. Bastos, M. Lundqvist, A. S. Waite, N. Kopell, E. K. Miller, Layer and rhythm specificity for predictive routing. *Proc. Natl. Acad. Sci. U.S.A.* **117**, 31459–31469 (2020).
60. N. T. Markov, J. Vezoli, P. Chameau, A. Falchier, R. Quilodran, C. Huissoud, C. Lamy, P. Misery, P. Giroud, S. Ullman, P. Barone, C. Dehay, K. Knoblauch, H. Kennedy, Anatomy of hierarchy: Feedforward and feedback pathways in macaque visual cortex. *J. Comp. Neurol.* **522**, 225–259 (2014).
61. Y. Yu, L. Huber, J. Yang, M. Fukunaga, Y. Chai, D. C. Jangraw, G. Chen, D. A. Handwerker, P. J. Molfese, Y. Ejima, N. Sadato, J. Wu, P. A. Bandettini, Layer-specific activation in human primary somatosensory cortex during tactile temporal prediction error processing. *Neuroimage* **248**, 118867 (2022).
62. T. A. Babola, S. Li, A. Gribizis, B. J. Lee, J. B. Issa, H. C. Wang, M. C. Crair, D. E. Bergles, Homeostatic control of spontaneous activity in the developing auditory system. *Neuron* **99**, 511–524.e5 (2018).
63. A. Attinger, B. Wang, G. B. Keller, Visuomotor coupling shapes the functional development of mouse visual cortex. *Cell* **169**, 1291–1302.e14 (2017).
64. T. S. Yarden, A. Mizrahi, I. Nelken, Context-dependent inhibitory control of stimulus-specific adaptation. *J. Neurosci.* **42**, 4629–4651 (2022).
65. T. Deneux, E. R. Harrell, A. Kempf, S. Ceballo, A. Filipchuk, B. Bathellier, Context-dependent signaling of coincident auditory and visual events in primary visual cortex. *eLife* **8**, (2019).
66. C. F. Doeller, B. Opitz, A. Mecklinger, C. Krick, W. Reith, E. Schröger, Prefrontal cortex involvement in preattentive auditory deviance detection: Neuroimaging and electrophysiological evidence. *Neuroimage* **20**, 1270–1282 (2003).
67. G. V. Carbajal, M. S. Malmierca, The neuronal basis of predictive coding along the auditory pathway: From the subcortical roots to cortical deviance detection. *Trends Hear* **22**, 233121651878482 (2018).
68. J. M. Cisneros-Franco, P. Voss, M. E. Thomas, E. de Villers-Sidani, Critical periods of brain development. *Handb. Clin. Neurol.* **173**, 75–88 (2020).
69. J. J. Huyck, B. A. Wright, Late maturation of auditory perceptual learning. *Dev. Sci.* **14**, 614–621 (2011).
70. A. B. Maxon, I. Hochberg, Development of psychoacoustic behavior. *Ear Hear.* **3**, 301–308 (1982).
71. D. R. Moore, J. A. Cowan, A. Riley, A. M. Edmondson-Jones, M. A. Ferguson, Development of auditory processing in 6- to 11-yr-old children. *Ear Hear.* **32**, 269–285 (2011).
72. F. Wightman, P. Allen, T. Dolan, D. Kistler, D. Jamieson, Temporal resolution in children. *Child Dev.* **60**, 611–624 (1989).
73. K. Banai, A. T. Sabin, B. A. Wright, Separable developmental trajectories for the abilities to detect auditory amplitude and frequency modulation. *Hear. Res.* **280**, 219–227 (2011).
74. R. K. Christensen, H. Linden, M. Nakamura, T. R. Barkat, White noise background improves tone discrimination by suppressing cortical tuning curves. *Cell Rep.* **29**, 2041–2053.e4 (2019).
75. E. Lu, D. A. Llano, S. M. Sherman, Different distributions of calbindin and calretinin immunostaining across the medial and dorsal divisions of the mouse medial geniculate body. *Hear. Res.* **257**, 16–23 (2009).
76. D. Choy Buentello, D. C. Bishop, D. L. Oliver, Differential distribution of GABA and glycine terminals in the inferior colliculus of rat and mouse. *J. Comp. Neurol.* **523**, 2683–2697 (2015).

77. T. Nath, A. Mathis, A. C. Chen, A. Patel, M. Bethge, M. W. Mathis, Using DeepLabCut for 3D markerless pose estimation across species and behaviors. *Nat. Protoc.* **14**, 2152–2176 (2019).
78. M. Pachitariu, N. A. Steinmetz, S. N. Kadir, M. Carandini, K. D. Harris, in *Advances in neural information processing systems,* D. D. Lee, M. Sugiyama, U. V. Luxburg, I. Guyon, R. Garnett, Eds. (NIPS Proceedings, 2016), pp. 4448–4456.
79. R. G. Natan, J. J. Briguglio, L. Mwilambwe-Tshilobo, S. I. Jones, M. Aizenberg, E. M. Goldberg, M. N. Geffen, Complementary control of sensory adaptation by two types of cortical interneurons. *eLife* **4**, e09868 (2015).
80. K. H. Pettersen, A. Devor, I. Ulbert, A. M. Dale, G. T. Einevoll, Current-source density estimation based on inversion of electrostatic forward solution: Effects of finite extent of neuronal activity and conductivity discontinuities. *J. Neurosci. Methods* **154**, 116–133 (2006).

Acknowledgments: We thank M. Solyga for assistance with the analysis, D. Machado for assistance with experiments, M. Nakamura for wild-type mouse order and transgenic lines breeding, and P. Scheiffele for providing Ntsr1-cre mice. **Funding:** This work was supported by the Swiss National Science Foundation (CRETP3-166735 and 310030-197850 grants). **Author contributions:** P.V. and T.R.B. designed the study, interpreted the data, and edited the manuscript. P.V. performed experiments, analyzed the data, and wrote the manuscript. J.R. consulted, developed code, and analyzed the data. S.J. and G.D.F. developed code for the data analysis. T.R.B. acquired the funding, supervised the project, and reviewed the manuscript. **Competing interests:** The authors declare that they have no competing interests. **Data and materials availability:** All data needed to evaluate the conclusions in the paper are present in the paper and/or the Supplementary Materials or available on Dryad (https://doi.org/10.5061/dryad.rn8pk0pj5).

Submitted 16 May 2023
Accepted 1 December 2023
Published 3 January 2024
10.1126/sciadv.adi7624